User's Guide

Approved for Unlimited Release, JPL CL#19-7345

Dataset name:
JPL MEASURES Gridded Sea Surface Height Anomalies Version JPL1812

Authors
Victor Zlotnicki (1), Zheng Qu (2), Joshua K. Willis (1), Richard Ray (3), Jessica Hausman (1)
(1) Jet Propulsion Laboratory, California Institute of Technology, Pasadena, CA, USA.
(2) Raytheon Corp., Pasadena CA, USA.
(3) NASA-Goddard Space Flight Center, Greenbelt, MD, USA

Abstract
Ocean topography gridded products from nadir satellite radar altimetry, distributed over the past nearly two decades by AVISO and now by CMEMS (Copernicus Marine Environment Monitoring Service) , have found a variety of applications, including eddy tracking, Antarctic Circumpolar Current fronts, and estimating the transport of the Atlantic Meridional Overturning Circulation among others. Nonetheless there was a need to update the gridding procedures, as certain simplifications imposed by historical computer restrictions are no longer necessary. This document describes a gridded data product produced at the Jet Propulsion Laboratory. This document describes both the "final" grids, with a delay of a few months, and the "interim" grids, produced in near real time. One key measure of quality of the resulting grids is a comparison to withheld altimetry data, not only in terms of overall root mean squared (RMS) discrepancy, but also assessing the spectral properties of grids versus withheld data. We find that these grids based on two satellites at any one time, reproduce wavelengths longer than 350 km near the Equator (4.3 cm RMS), 150 km in the Antarctic Circumpolar Current region (4.0 cm RMS), and 250 km in the Gulf Stream region (9 cm RMS). Another quality measure is by comparison with a set of 61 well distributed, high quality tide gauges, with inverted barometer applied; we find that the standard deviation of the detrended difference between our grids and the tide gauges is 3.1 cm, while the standard deviation of the tide gage time series is 7.5 cm. The above assessment applies to the "final" grids; there is an overall RMS difference of 2.5 cm between final and interim grids.

Credit
Please cite these data as:

Zlotnicki V., Z. Qu, J. Willis. R. Ray and J. Hausman. 2019 JPL MEASURES Gridded Sea Surface Height Anomalies Version 1812. PO.DAAC, CA, USA. Dataset accessed [YYYY-MM-DD] at https://doi.org/10.5067/SLREF-CDRV2

Indicating whether you used the final or interim grids.

Introduction

In a series of papers (LeTraon et al, 1998; Ducet et al, 2000; LeTraon and Dibarboure, 2002), P.Y. LeTraon and colleagues established an efficient and accurate method to grid sea surface heights (SSH) from time-varying alongtrack nadir radar altimeter data using objective mapping (Bretherton et al., 1976); they paid special attention to the removal of long wavelength alongtrack error, and ascertained the accuracy of the technique by sampling numerical model output in the manner a nadir altimeter does, gridding the sampled model, and compared to the full model grids. The latest version of that series is discussed in Pujol et al (2016). The grids produced by various versions of their technique by SSALTO/DUACS and distributed by AVISO sponsored by the Centre Nationale d' Etudes Spatiales of France have been widely used. The data are now distributed by the Copernicus Marine Environment Monitoring Service, CMEMS, https://marine.copernicus.eu. For example Chelton et al (2011a) used them to track nonlinear mesoscale eddies based on closed contours of SSH, itself a data product later used in other studies (e.g. Chelton et al, 2011b; Samelson et al, 2014); Willis (2010) demonstrated that the SSH maps together with Argo data showed skill in estimating the transport of the upper limb of the Atlantic Meridional Overturning Circulation around 41^{o}N; Sokolov and Rintoul (2007) and Thompson and Sallé (2012) used those grids to study fronts of the Antarctic Circumpolar current. This list is just a very small sample of the many applications those maps have found.

Despite their success, AVISO also saw the need to update certain choices made long ago in the gridding procedure, and released a new set of grids in 2014, labelled DT2014 (Pujol et al, 2016).

The set of grids described here use a technique similar to objective mapping, called simple krigging (https://en.wikipedia.org/wiki/Kriging; Cressie and Wikle, 2011, chapter 4). The details are described below

Input Data.

All grids are constructed from two simultaneous altimetric satellites. One satellite is one of TOPEX/Poseidon (T/P), Jason-1, Jason-2, or Jason-3. The other satellite is one of: ERS-1, ERS-2, Envisat, AltiKa, Cryosat-2, and now Sentinel 3A. Data from the first set are obtained from the alongtrack data product generated by the Goddard Space Flight Center (GSFC) and distributed by PO-DAAC, entitled **Integrated Multi-Mission Ocean Altimeter Data for Climate Research, version 4.2.** Note that T/P data in version 4.2 has the Wallops correction 'un-applied', which partially corrects an error in the early years of the mission (Beckley et al, 2017). At the time of this writing, T/P retracking and reprocessing is under way and the global mean sea level curve during the TOPEX era is likely to change ~1cm or less after reprocessing is complete. The data for the second set of satellites is obtained from the RADS database (*http://rads.tudelft.nl, https://github.com/remkos/rads/tree/master/doc/manuals*) with default corrections as of October 2018. The exact satellites used depend on the date, as described in the table below.

Date	Satellite 1	Date	Satellite 2
19920923 to 20020514	TOPEX/Poseidon	19920923 to 19950425	ERS-1
20020514 to 20080704	Jason-1	19950425 to 20020514	ERS-2
20080702 to 20160212	Jason-2	20020514 to 20100714	Envisat
20160212 to present	Jason-3	20101024 to 20130314	CryoSat-2
		20130314 to 20160704	AltiKa
		20160704 to Present	Sentinel 3A

Method.

First, the input data is smoothed with a 19-point filter: the filter is a sinc function multiplied by a Blackman window, with cutoff frequency of 0.11 Hz. The coefficients used are listed below (the filter is symmetric, and values below are for right-side coeeficients, starting from the center point coefficient, to the rightmost one):

[0.222115, 0.196706, 0.134041, 0.0646945, 0.0150775, -0.00675300, -0.00907955, -0.00461792, -0.00110582, -2.06117e-05]

See the plots below for the filter response against simulated altimeter data. The “RADS smoothed” (2nd panel from top) signal is constructed out of a random RADS track, using a low pass Butterworth filter (see filter response function at top panel) with cutoff around 0.1 HZ (10 points). A random noise with 6cm STDev is added to the “RADS smoothed” to create simulated altimeter data to test the filter response.

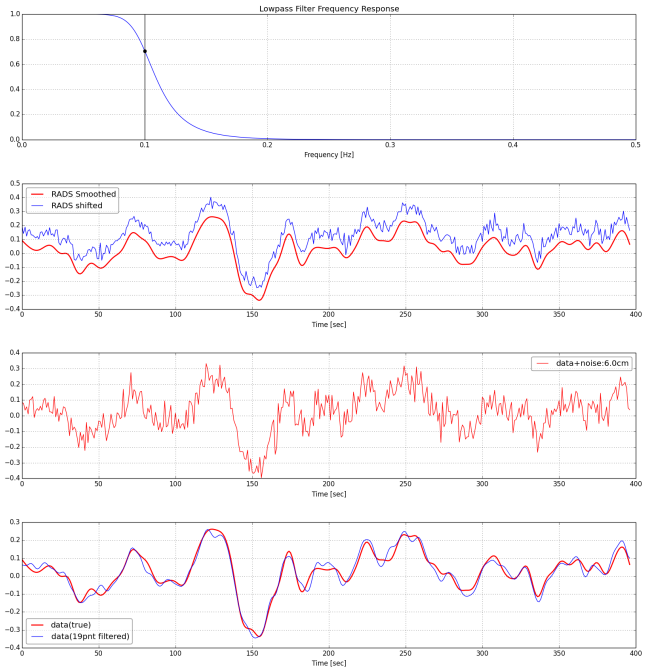

Next, for each satellite series, a daily global mean sea surface level (GMSL) is computed using the smoothed input data, h'(x,y, t) , following Wang (OSU report 430); Parke et al (1987). Let's denote them as $GMSL_1(x,y, t)$ and $GMSL_2(x,y, t)$, respectively for Satellite 1 and 2, where Satellite 1 is from the TOPEX/Jason series, produced by GSFC. The daily value of $GMSL_1$ and $GMSL_2$ is computed each as a mean for 19 days (centered at the desired date for the daily GMSL) worth of input data. The daily input data from Satellite series 2, denoted as $h_2(x,y, t)$, is adjusted such that $GMSL_2$ will match $GMSL_1$:

$$h_2(x,y, t) = h'_2(x,y, t) * GMSL_1(x,y, t) / GMSL_2(x,y, t)$$

Then, a covariance function for each location over the global oceans was obtained as follows. The analytical function

$$C_{ij} = var*b*\exp(-a*r_{ij} - (dt_{ij}/Lt)^2) = \langle h(x_i,y_i,t_i)h((x_j,y_j,t_j)\rangle$$

is used, where:

< > is an expected value operator, implemented as average over pairs separated by the same dx, dy, dt
h(x,y,t) is the sea surface height at horizontal position x,y, time t,
Lt= 10 days for latitudes up to 5°, 15 days for latitudes higher than 10°, and linearly in between
$a = 3.3369, \quad b = 1 + r + r^2/6 - r^3/6$
$r = \sqrt{(((dx-Cx*dt)/Lx)^2 + ((dy-Cy*dt)/Ly)^2)}$, $dx=x_i-x_j$, likewise for dy and dt.

var = squared root mean squared h from TOPEX and Jason alongtrack data 1993-2014.

Lx and Ly are length scales in the zonal and meridional directions determined by fitting the above function to alongtrack covariance functions determined from historical alongtrack repeat altimetry data along the TOPEX and Jason-1 and -2 tracks, then rotated using Jacobs (2013) estimate of the ratio of zonal and meridional length scales.

Cx and Cy are drift velocity components, determined as follows: in a first step, Cx, Cy are set to zero and the complete dataset is used to generate grids sampled every 1/6 degree and 5 days. In a second step, Cx and Cy are determined from successive grids by decomposing into circles, whose radius is the zero crossing of the correlation function (Figure 2), shifting two corresponding boxes by 1 degree offset in all directions, and computing their correlation coefficient, finally determining Cx and Cy from the relative position of the two boxes with maximum cross correlation. The final step reruns the whole gridding computation using the Cx and Cy maps thus determined.

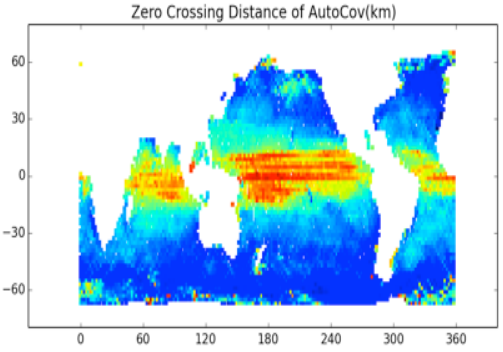

Figure 2: zero crossing distance of the autocovariance function, estimated from alongtrack altimetry data.

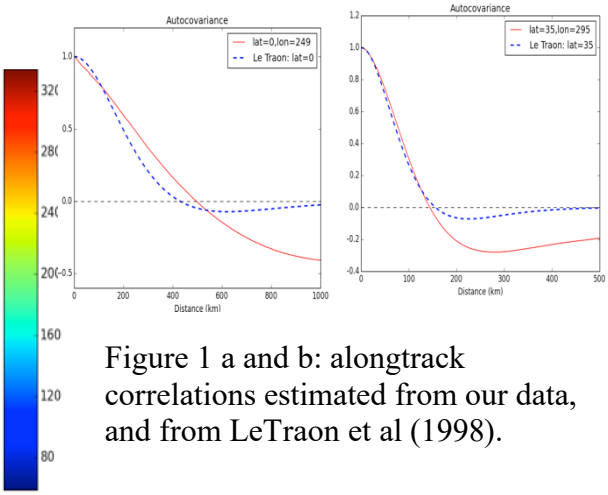

Figure 1 a and b: alongtrack correlations estimated from our data, and from LeTraon et al (1998).

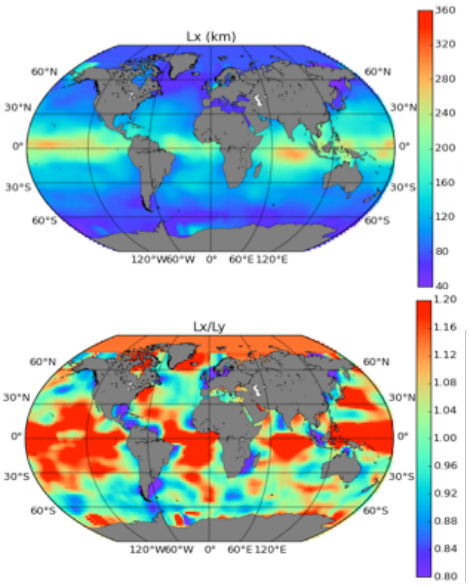

Figure 3: Top: Lx from Greg Jacobs, 2014, pers. Comm.. Bottom: the ratio Lx/Ly from the same source.

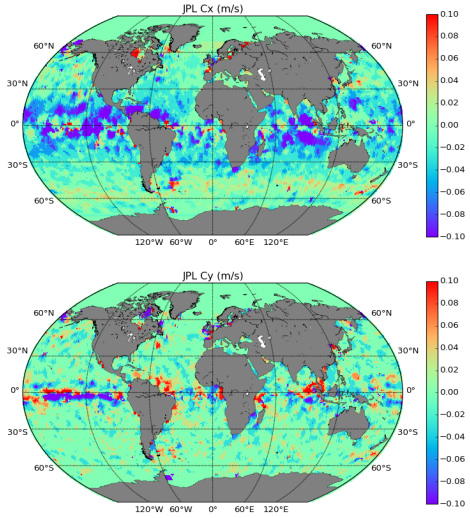

Figure 4: propagations velocity components Cx and Cy for 2010-01-05 (a new set of Cx, Cy is computed for each 5 day map).

Given the above covariance function, the estimation of h(P), P=(x,y,t) is the linear combination h(P)= sum(h(Q_i)w_i(P,Q_i))
where the vector w of weights w_i is estimated by least squares as

$$\begin{bmatrix} w \\ \mu \end{bmatrix} = \begin{bmatrix} D & 1 \\ 1 & 0 \end{bmatrix}^{-1} \begin{bmatrix} C \\ 1 \end{bmatrix}$$

where C is the set of C_{ij} between the position of interpolation i (grid node) and each of the surrounding data points j ; D=C'+E is the sum of the matrix of C'_{ik} between any two data points i and k and the expected error covariance E_{ik} between those two positions. E_{ik} is diagonal, except

when two data points are on the same groundtrack, where a bias error is allowed and solved for. This track bias is assumed to be (1cm)^2 for the TOPEX, Jason-1,-2, -3 satellites, and (3cm)^2 for the ERS-1, -2, Envisat, AltiKa satellites.

To avoid combining data in different 'correlation zones' (for example, Atlantic and Pacific across Panama), 'zones' were defined, see map below. Solid color zones cannot combine data with another color zone, but can combine with white. Dotted color zones cannot combine with any other zone.

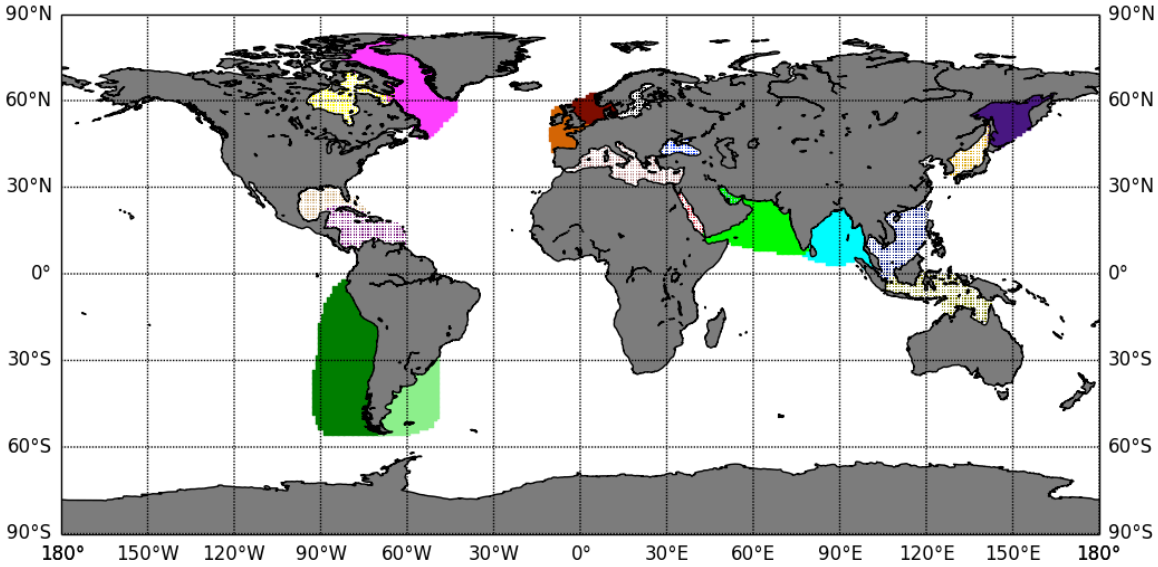

The matrices do not contain all the global data distribution, but only data in two windows: the inner window has a 400 km radius, the outer window 1050km radius, the time window 30 days. All data in the inner window are used, 1 data point every 3 in the outer window are used. The matrix is inverted for all points inside a 1° box in both latitude and longitude to compute weight vector *w*.

After obtaining grid values h(P) following the aforementioned steps, a cosine latitude weighted global mean sea level value, GMSL3, is computed daily using 1 day's worth of grid values. The grid values are further adjusted such that the output GMSL3 matches the GMSL1:

$h(P)' = h(P) * GMSL1/GMSL3$

Finally, a time mean map, using grids from 1993 up to the latest whole year (which is 2018 as of Feb 2019) is computed and subtracted from grid values to generate the final data product, e.g.,

$h_{final} = h' - h_{mean\_1993\_2018}$

Accuracy Assessment against altimetry.
Accuracy has been assessed by withholding data from one altimeter (of the T/P, J-1, J-2 series) for one day, then comparing the resulting grids to the withheld data. This produces an upper bound on the error, since the final grids include all data. The data were compared both spatially

and spectrally. The figures below show the spatial power spectrum of the withheld alongtrack data, of the gridded product interpolated linearly to the position of the alongtrack data, and the spectrum of the difference. See caption for details.

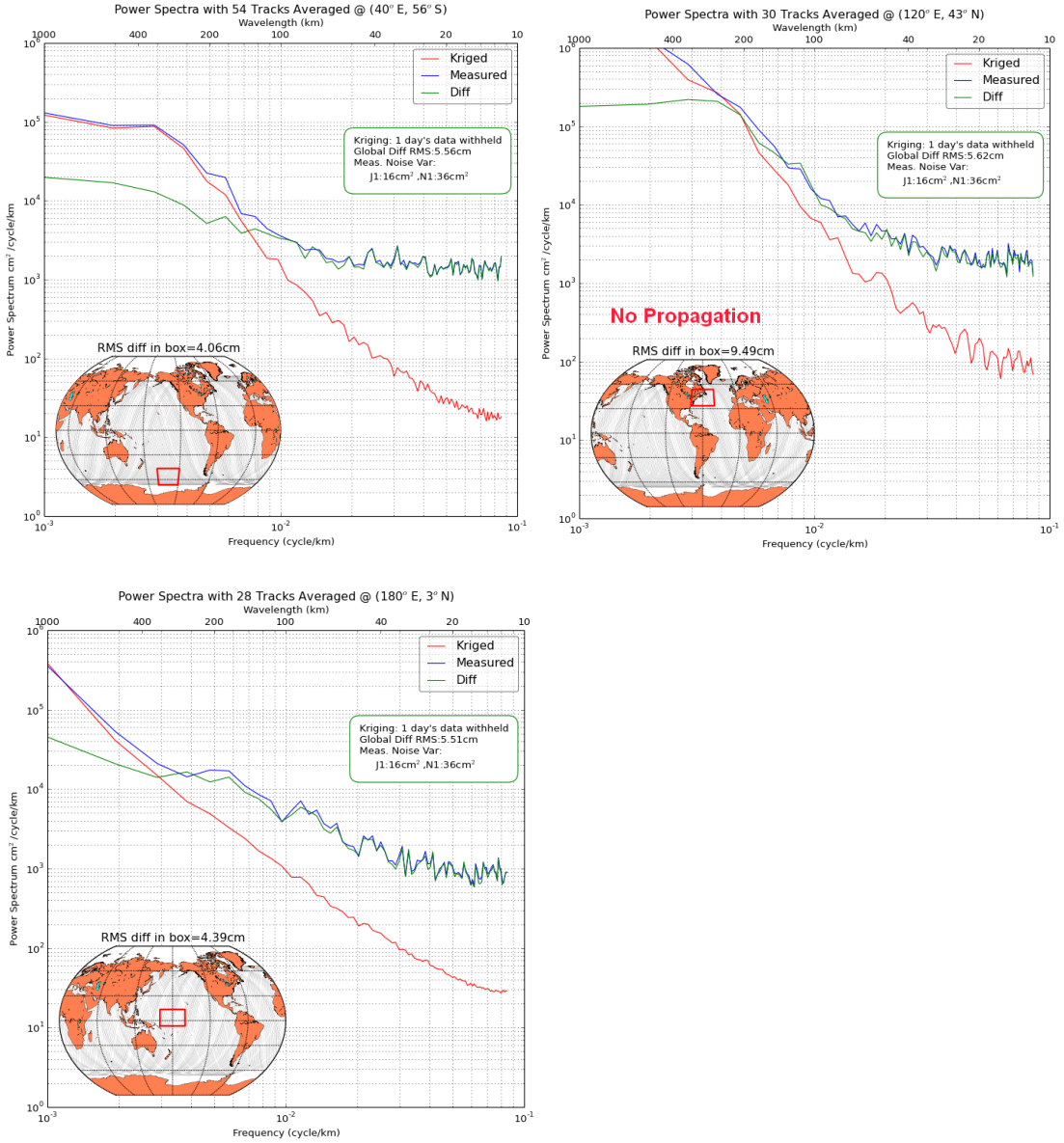

Figure 5: spectra of withheld alongtrack T/P or J-1 or J-2 data, spectra of the map without these data, interpolated to the time and position of the alongtrack data, and spectra of the difference. As can be seen, the interpolation retrieves in the ACC region wavelengths longer than 150km with 4 cm overall RMS, in the Gulf Stream region wavelengths longer than 225km with 9.5 cm RMS, and in the equatorial region wavelengths longer than 350km with 4.4 cm RMS.

We have not carried out a detailed error assessment near coasts, where altimeter errors increase, either due to land contamination of the radiometer or altimeter, or increased uncertainty of the tidal correction, or the fact that data from deeper water are included in the interpolation due to the search radii and the absence of data on one side of the search box. Users are urged caution in interpreting near coastal data. The authors would welcome any findings on their accuracy (please email victor.zlotnicki[at]jpl.nasa.gov).

Accuracy assessment against tide gauges. (TBD: revise with Richard's new plots)

The grids were compared against a set of 61 tide gauges with long time series covering the period of the grids (Richard Ray, 2016, pers. Comm.). The distribution of the tide gauges is shown in figure 6, while a few time series are shown in figure 7.

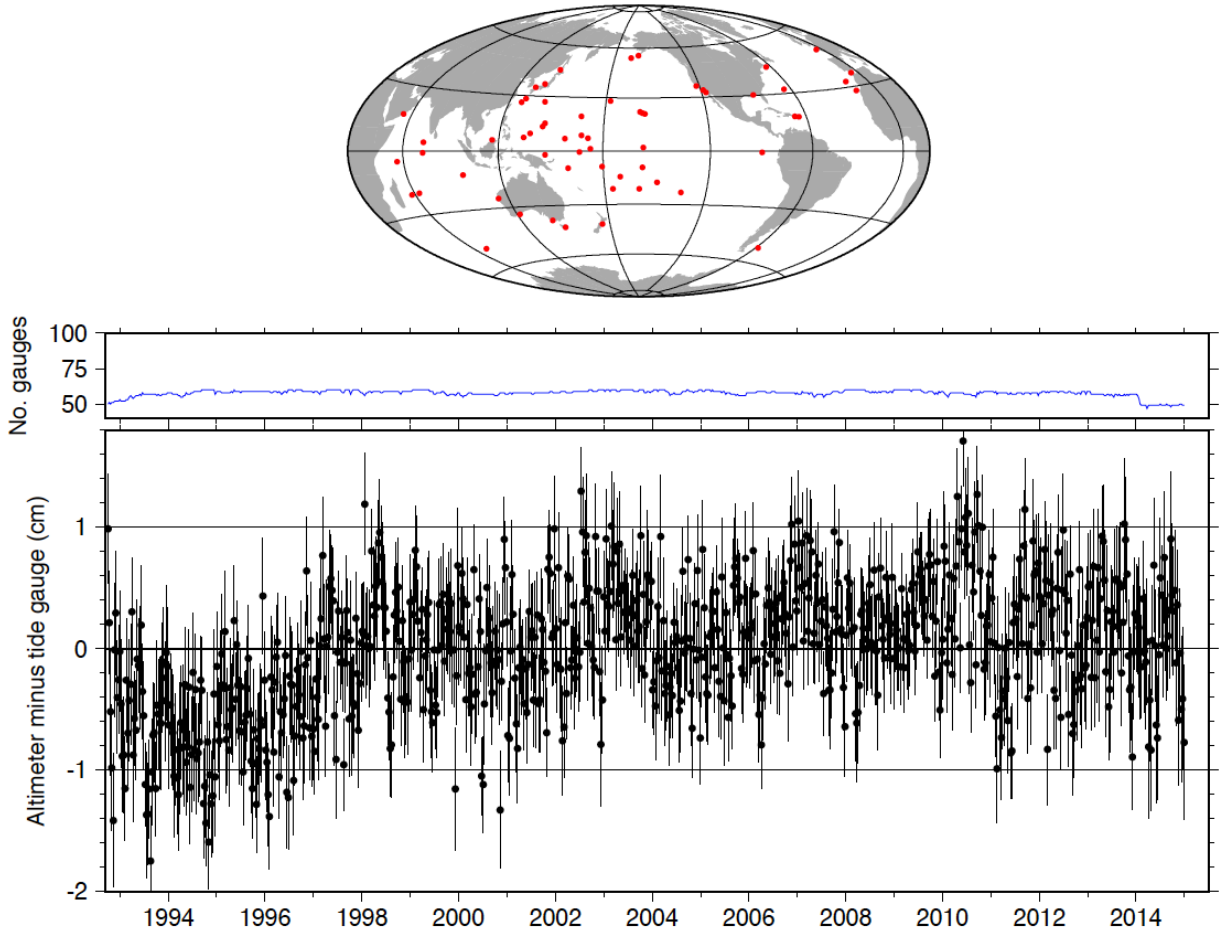

Figure 6: (TOP) spatial distribution of the 61 tide gauges used in this comparison. Bottom: global average of the difference between altimetric grid and tide gauges. The 'drop' before 1998 is a well-known feature related to an inaccurate TOPEX correction, which has been corrected in the current grids.

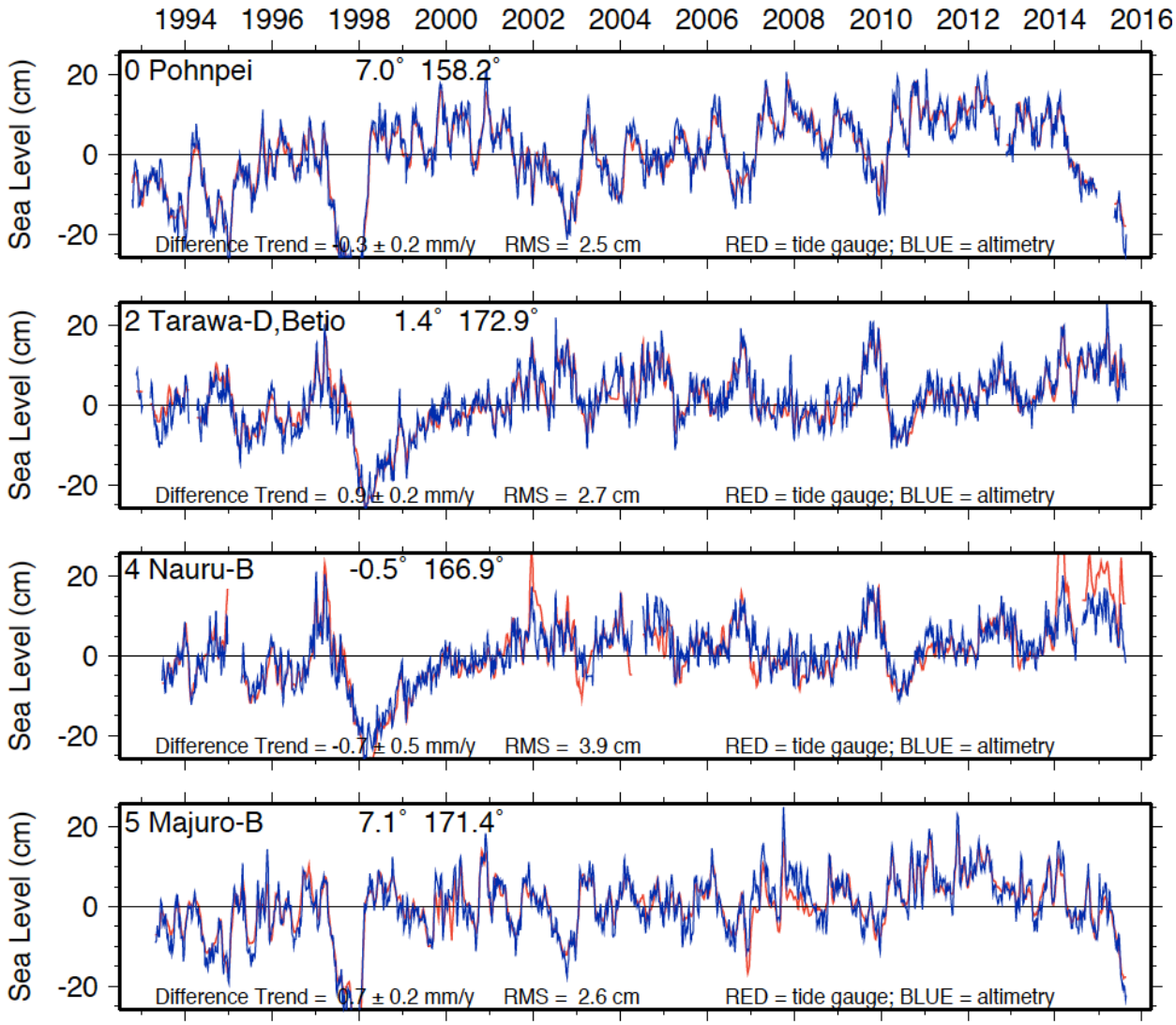

Figure 7. Sample time series of altimetric grid (blue) and tide gauge (red). Note the excellent agreement; the discrepancy at the end of the Nauru time series has been found to be a tide gauge error.

The combined standard deviation (SD) of the tidegauges is 7.5 cm, the SD of the detrended difference between JPL altimetry and tide gauges is 3.1 cm. We also compared the latest version of the AVISO 2-satellite grids to the same set of tide gages. The SD of their difference was 2.5 cm. The nature of the difference is associated with short period noise in the JPL grids.

Difference between "final" and "interim" grids

The difference between "final" grids, computed exactly as described above, and "interim" grids is this: the data source for the Jason series of satellites instead of being the Goddard Space Flight Center processed data, which is usually delayed by a few months in order to yield the highest accuracy product, is obtained from the RADS system in near real time. The difference between

these two sets of grids is illustrated in Figure 8, with a globally-averaged root mean squared difference of 25 mm.

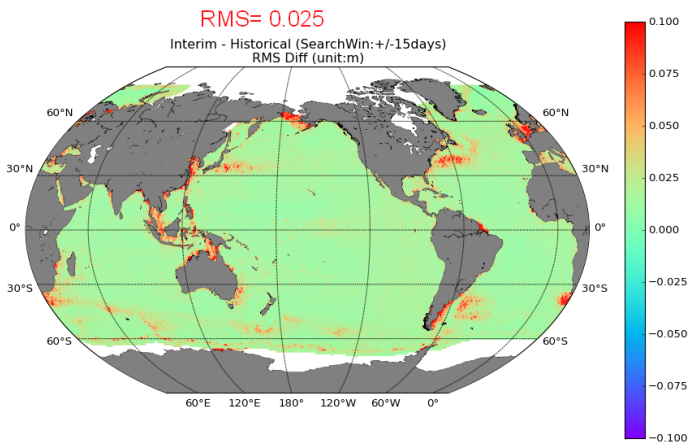

Figure 8. RMS difference between "final" and "interim" grids

Coverage and resolution:
The grids are given every 5 days and 1/6 degree spatial sampling. The actual resolution is as illustrated in the "accuracy assessment" section.

Format:
The filenames are of the form ssh_grids_v1812_1992100712.nc , where the date of the midpoint of the interpolation is year 1992, month 10, day 07, hour 12 noon. The extension 'nc' refers to the netCDF format. The interim grids are identified by the string '_i' following the date in the filename, as in ssh_grids_v1812_1992100712_i.nc. The version id refer to the year and month when the code was frozen.

The data files are netCDF, CF compliant. The attributes can be seen below:

File "ssh_grids_v1812_2018042912.nc"

File type: NetCDF-3/CDM

```
netcdf file:/Users/vzl/Desktop/ssh_grids_v1812_2018042912.nc {
  dimensions:
    Time = UNLIMITED;   // (1 currently)
    Longitude = 2160;
    Latitude = 960;
    nv = 2;
  variables:
    float Lon_bounds(Longitude=2160, nv=2);
      :units = "degrees_east";
      :comment = "longitude values at the west and east bounds of each
pixel.";

    float Lat_bounds(Latitude=960, nv=2);
```

```
      :units = "degrees_north";
      :comment = "latitude values at the north and south bounds of each
pixel.";

    float Time_bounds(Time=1, nv=2);
      :units = "Days since 1985-01-01 00:00:00";
      :comment = "Time bounds for each time value, same value as time
variable. The time variable is defined on points instead of on bounding
boxes.";

    float SLA(Time=1, Longitude=2160, Latitude=960);
      :units = "m";
      :long_name = "Sea Level Anomaly Estimate";
      :standard_name = "sea_surface_height_above_sea_level";
      :coordinates = "Time Longitude Latitude";
      :alias = "sea_surface_height_above_sea_level";

    float SLA_ERR(Time=1, Longitude=2160, Latitude=960);
      :units = "m";
      :long_name = "Sea Level Anomaly Error Estimate";
      :coordinates = "Time Longitude Latitude";

    float Longitude(Longitude=2160);
      :standard_name = "longitude";
      :units = "degrees_east";
      :point_spacing = "even";
      :long_name = "longitude";
      :axis = "X";
      :bounds = "Lon_bounds";
      :_CoordinateAxisType = "Lon";

    float Latitude(Latitude=960);
      :standard_name = "latitude";
      :units = "degrees_north";
      :point_spacing = "even";
      :long_name = "latitude";
      :axis = "Y";
      :bounds = "Lat_bounds";
      :_CoordinateAxisType = "Lat";

    float Time(Time=1);
      :standard_name = "time";
      :long_name = "Time";
      :units = "Days since 1985-01-01 00:00:00";
      :calendar = "gregorian";
      :bounds = "Time_bounds";
      :axis = "T";
      :_CoordinateAxisType = "Time";

  // global attributes:
  :Conventions = "CF-1.6";
  :ncei_template_version = "NCEI_NetCDF_Grid_Template_v2.0";
  :Institution = "Jet Propulsion Laboratory";
  :geospatial_lat_min = -79.916664f; // float
  :geospatial_lat_max = 79.916664f; // float
  :geospatial_lon_min = 0.083333336f; // float
  :geospatial_lon_max = 359.91666f; // float
```

```
  :time_coverage_start = "2018-04-29";
  :time_coverage_end = "2018-04-29";
  :date_created = "2019-02-11T20:51:46.107133";
  :version_number = "1812";
  :summary = "Sea level anomaly grids from altimeter data using Kriging
interpolation, which gives best linear prediction based upon prior knowledge
of covariance. ";
  :title = "Sea Level Anormaly Estimate based on Altimeter Data";
  :_CoordSysBuilder = "ucar.nc2.dataset.conv.CF1Convention";
```

Acknowledgements

The research was carried out in part at the Jet Propulsion Laboratory, California Institute of Technology, under a contract with the National Aeronautics and Space Administration (80NM0018D0004).

References

Beckley, B.D, P.S. Callahan, D. W. Hancock III, G. T. Mitchum and R. D. Ray (2017): On the "Cal-Mode" Correction to TOPEX Satellite Altimetry and Its Effect on the Global Mean Sea Level Time Series, J. Geophys. Res – Oceans, https://doi.org/10.1002/2017JC013090. See also the poster at https://mediatum.ub.tum.de/doc/1523987/file.pdf

Bretherton, F., R. Davis and C. Fandry (1976). A technique for objective analysis and design of oceanographic experiments, applied to MODE73. Deep Sea Research, v23, pp 559-582.

Cressie N. and C.K.Wikle (2011) Statistics for spatio-temporal data. J. Wiley. ISBN-13: 978-0471692744

Ducet, N., P.-Y. Le Traon, and G. Reverdin, 2000: Global highresolution mapping of ocean circulation from TOPEX/Poseidon and ERS-1 and-2. J. Geophys. Res., 105, 19 477–19 498, doi:10.1029/2000JC900063.

Dudley B. Chelton ⇑, Michael G. Schlax, Roger M. Samelson, 2011a Global observations of nonlinear mesoscale eddies Progress in Oceanography 91 (2011) 167–216, doi:10.1016/j.pocean.2011.01.002

Dudley B. Chelton, Peter Gaube and Michael G. Schlax, 2011b The Influence of Nonlinear Mesoscale Eddies on Near-Surface Oceanic Chlorophyll. Jeffrey J. Early, Roger M. Samelson, Science, vol 334, pp 328-332, doi 10.1126/science.1208897

Le Traon, P-Y and G. Dibarboure 2002 Velocity Mapping Capabilities of Present and Future Altimeter Missions: The Role of High-Frequency Signals JTECH vol 19, pp 2077-2087,

Le Traon, P-Y, F. Nadal, and N. Ducet, 1998 An Improved Mapping Method of Multisatellite Altimeter Data J. of Atmospheric and Oceanic Techn, Vol 15, p522-534,

Pujol, M.-I., Y Faugere et al (2016): DUACS DT2014: the new multimission altimeter data set reprocessed over 20 years. Ocean Sci., 12, 1067-1090. doi:10.5194/os-12-1067-2016

Samelson, R.M., M. G. Schlax, And D. B. Chelton, 2014 Randomness, Symmetry, and Scaling of Mesoscale Eddy Life Cycles JPO vol 44, pp 1012-1029. DOI: 10.1175/JPO-D-13-0161.1

Scharroo, R., E. Leuliette, M. Naeije, C. Martin-Puig, and N. Pires (2016). RADS Version 4: An Efficient Way to Analyse the Multi-Mission Altimeter Database, Living Planet Symposium, Proceedings of the conference held 9-13 May 2016 in Prague, Czech Republic. Edited by L. Ouwehand. ESA-SP Volume 740, ISBN: 978-92-9221-305-3, p.428

Sokolov, S., and S. R. Rintoul, 2007 Multiple jets of the Antarctic Circumpolar Current south of Australia. J. Phys. Oceanogr., 37, 1394–1412.

Thompson, Andrew F.and Jean-Baptiste Sallee´ (2012) Jets and Topography: Jet Transitions and the Impact on Transport in the Antarctic Circumpolar Current JPO vol 42, p 956-972, DOI: 10.1175/JPO-D-11-0135.1

Wunsch, C., and V. Zlotnicki, 1984: The accuracy of altimetric surfaces. Geophys. J. Royal. Astron. Soc., 78, 795–808.